Renewable Energy 226 (2024) 120413

Contents lists available at ScienceDirect

Renewable Energy

journal homepage: www.elsevier.com/locate/renene

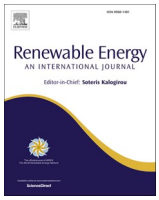

An experimental study of the thrust and power produced by a 1/20th scale tidal turbine utilising blade winglets

Rodolfo Olvera-Trejo *, Luke Myers, Luke Blunden, AbuBakr S. Bahaj

Energy and Climate Change Division, Faculty of Engineering and Physical Sciences, University of Southampton, University Road, Southampton, SO17 1BJ, United Kingdom

ARTICLE INFO

Original content: Winglets (Original data)

Keywords:
Experimental
Flow visualisation
Marine energy
Tidal turbine
Winglets

ABSTRACT

Winglets have been employed in the aviation industry to reduce vortices generated at aircraft wings, decreasing drag, and hence increasing fuel economy. For rotating applications previous experimental and numerical studies addressed the application for wind turbines and suggested winglets facing backwards on the suction side of a blade could increase the power capture. This paper presents experimental work using a scale 3-bladed horizontal axis tidal turbine. An oil-based paint flow visualisation coupled to blade thrust and torque measurements helped to identify the mechanism behind the phenomenon affecting the performance of winglets facing the suction side of a turbine blade. The results show that on average a winglet facing downstream decreases the power coefficient 1–2% and increases the thrust coefficient up to 6% for tip speed ratios 5.0–7.0. On the other hand, a symmetrically mirrored winglet facing upstream increased the power coefficient by 1–2%, and the thrust coefficient by 3–4%. Winglets have the potential to provide a meaningful increase to power capture at minimal additional capital cost without increasing rotor diameters. Further work to optimize pressure-side winglets should be conducted.

1. Introduction

Globally there are ongoing activities with targets geared to decarbonise our electricity generation. Many countries have set targets to achieve an ever-increasing share of electricity production from renewable energy sources to alleviate the emissions emanating from fossil fuel use. More recently an additional-urgency to move to low -carbon sources was brought into sharper focus by global geopolitical events – such as the war in Ukraine and its effect on gas supplies. Wholesale prices for gas and electricity have increased sharply from relatively stable levels and national governments are now taking security of supply much more seriously and as a driver to develop indigenous sources of renewable energy electrical power generation. Previously, the EU Renewable Energy Directive [1] set a target of 20% renewables by 2020 on average between member states which was recently revised upwards to 45% by 2030 [2]. Similarly, the UK had a target of 30% of its electricity to be produced from renewables by 2020 [1], which was achieved and exceeded in 2019, where 35% of total electricity generation came from renewables. More recently, the UK announced an intention of achieving 95% of its electricity from low-carbon sources by 2030, with high dependence on offshore wind, solar energy, and nuclear power to support electricity supply independence and security [3].

Marine energy, specifically that which arises from the kinetic energy of the flow in the oceans (tidal stream and ocean currents), can contribute to renewable energy capacity, and increase diversity of generation [4]. Tidal stream is also highly predictable so that power generation can be smoothly integrated in power grids delivery at scale. However, as this is an emerging technology, it will need clear support mechanisms to achieve a reduction in the presently high Levelised Cost of Energy (LCOE) so that it can compete with other renewables [5].

At the time of writing and in many countries, the support for marine energy technologies is somewhat uncertain. However, recently the UK Government has provided a ring-fenced funding support mechanism for marine energy in its fourth round of the Contracts for Difference (CfD). The CfD funding guarantees a fixed price for electricity from renewables supplied to the national grid. In July 2022 under the UK CfD scheme, it was announced that four free stream tidal energy projects with a total installed capacity of 40.82 MW, at CfD price of £178.54/MWh will be supported [6]. This must be seen in the context of a historical market price of approximately £50/MWh since 2010 as compared to 2022

* Corresponding author. Energy and Climate Change Division, Faculty of Engineering and Physical Sciences, University of Southampton, SO16 7QF, Southampton, United Kingdom.
E-mail address: R.Olvera@soton.ac.uk (R. Olvera-Trejo).

https://doi.org/10.1016/j.renene.2024.120413
Received 7 February 2023; Received in revised form 1 March 2024; Accepted 28 March 2024
Available online 1 April 2024

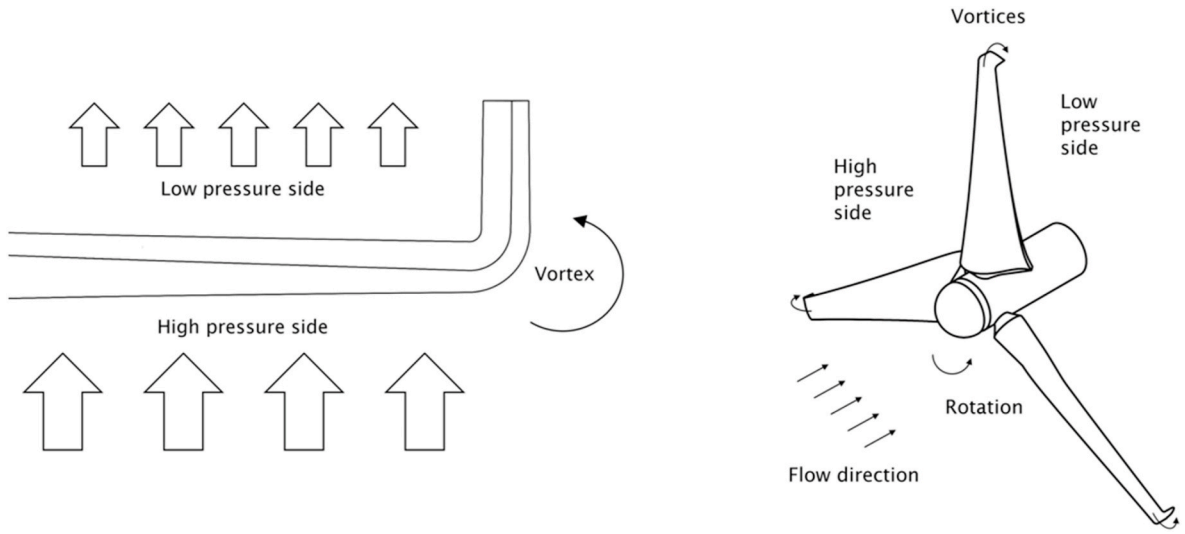

Fig. 1. Left: Vortex direction on an airplane wing. Right: Tip vortices on a tidal turbine.

where the level is currently in the range £150 to £250/MWh as a result of market price volatility.

There have been several deployments of sizeable tidal turbines to date with a latter move to small grid-connected farms or arrays of multiple devices. The European Marine Energy Centre (EMEC) in Orkney, UK, maintains grid-connected testing berths currently serving large-scale prototype devices. The most advanced projects at the time of writing are the Shetland tidal array located in Bluemell sound consisting of four 100 kW devices and the Meygen project located in the Inner Sound of the Pentland Firth presently consisting of four devices with total rated power of 6 MW. There are numerous areas in waters around the British Isles and indeed worldwide with consents and permissions granted for freestream tidal energy projects. The €46.8m TIGER project funded by the European Interreg programme has a stated aim to support the tidal industry to reduce costs from an estimated €300 MW/h to €150 MW/h by 2025 [7] as well as provide support for up to 8 MW of installed capacity at sites around the Channel region between the UK and France.

Reducing the LCOE can be achieved by reducing the capital cost of the turbines in combination with maximising power generation through increased efficiency of energy conversion that can arise from optimising the power capture, power-take-off and electrical subsystems. One significant gain can be made from the primary power-capture subsystem which in most cases for a tidal turbine is a lift force-based rotor. Common routes such as increasing rotor diameter or constructing thinner more slender blades are naturally limited due to the high thrust forces per unit area and the constrained depth of tidal sites.

Winglets of different designs have been employed extensively in the aviation sector and now most new modern commercial aircraft have winglets present at the wing tips. Enercon, to the best of the authors' knowledge, is the only wind turbine manufacturer that has invested in research that has led to winglets being used on its most recent designs [8]. However, to our knowledge there is no available performance data is made available in the public domain. In implementing winglets to a turbine blade, blade root and tip losses are two areas that will require attention with regard to increasing power capture. Further, Enercon has recently deployed blades that extend onto the hub nose cone (with flow-directing surfaces on the nose cone itself) to minimise hub losses and winglets at the blade tips to minimise or even negate aerodynamic tip losses.

This work focuses on the design and quantification of performance of winglets installed on a 1-m diameter model tidal turbine. The work investigates the advantages of winglets for a tidal turbine to increase power capture for the same rotor diameter through a blade modification that has a relatively modest cost, thus reducing the LCOE with minimal change to the overall device design.

2. Review of winglet design, application and research

Throughout the years, different methods have been proposed to increase energy extraction from turbine blades using techniques such as: micro-tabs, non-straight blades, winglets, passively adaptive blades, slots, and tubercles. The most widely studied type, and probably the ones that have shown better results on aeroplane wings, are winglets. In 1897, the English engineer Frederick W. Lanchester obtained a patent for vertical surfaces at the wing tips. In 1976 an aeronautical engineer, Richard Whitcomb, conducted research at NASA using the term winglet to refer to a nearly vertical wing extension in order to reduce the induced drag on wings [9]. In principle, the winglets' main function is to prevent the interaction from the high to the low-pressure sides of the wing, reducing the tip vortex, whilst decreasing the spanwise flow, resulting in reducing the induced drag [10]. Fig. 1 (Left) shows the vortex formed at the edge of a wing where the flow from the high-pressure side travels towards the low-pressure side, as a result of the pressure difference. Fig. 1 (Right) illustrates the same vortices occurring at the turbine blade tips. In contrast to an aeroplane wing, where vortices are perpendicular to the stream flow, for rotating turbines (wind or tidal), the vortices travel in the same direction as the fluid.

Early work, in 1985 [11], which tested tip devices on a horizontal axis wind turbine found no apparent improvement over the regular wing performance. The work emphasized that *'The promising results obtained on nonrotating wings make it difficult to accept that tip devices could not improve wind turbine performance'*. Mie University, in collaboration with Delft University of Technology (DUT), carried out a series of experiments on "Mie-type" winglets [12]. The "Mie-type" vanes of approximately 20% of the height of the blade were tested and an increase in the power coefficient (C_p) of around 27% for a blade Tip Speed Ratio (TSR) of 4 was reported. After that, Van Bussel [13] developed a momentum theory for a blade-winglet configuration. The main assumption was that the increase in power was due to the shift in the vorticity of the wake downstream. Further experiments and an adjusted theoretical model were then reported showing a 17% increase in power coefficient for a tip speed ratio of 5. Other studies in 2003 were conducted and a power augmentation of 8.75% was reported [14].

Later in 2006/07 Johansen, Sørensen and Gaunna [15] used Computational Fluid Dynamics (CFD) to investigate the possible increase in C_P by using winglets on wind turbines tested at Risø National Laboratory, Denmark.A key aspect of their study was the utilisation of the geometry described by Maughmer [10] which defined 8 key

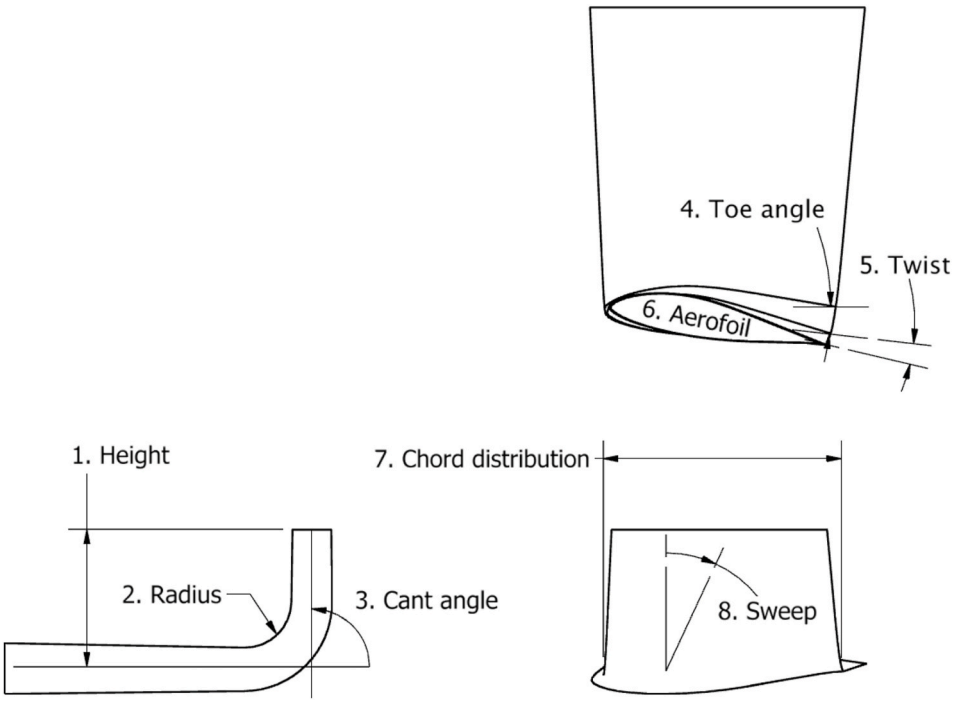

Fig. 2. Winglet geometry design variables.

geometric parameters of winglets: height (relative to the blade length), radius of curvature (relative to the winglet height), cant angle,[1] toe angle, twist, aerofoil, chord distribution and sweep (Fig. 2). Their initial study using the general-purpose incompressible Navier Stokes-solver EllipSys3D on winglets 1.5% (of blade length) high, a cant angle of 90°, and a sweep angle of 0° concluded that winglets could increase power coefficient by 1.3% while increasing the thrust coefficient 1.6% for the best configuration, that winglets affect approximately the outer 14% of the blade, and that winglets facing downstream performed better. Further work by the same group using the same solver, provided analyses of 10 winglets facing downstream, with heights varying from 1 to 4%, curvature, radii 12.5–100%, twist angle up to 8°, and one with a sweep angle of 30°. They found an increase in power of around 1.2%–2.8%, with an increase in thrust coefficient (C_T) of 1.2%–3.6% [16]. The study concluded that the power augmentation was a consequence of a reduction of tip effects, and not caused by the shift on downwind vorticity as it was believed until then. The idea that downwind winglets were superior was still supported. The studies were conducted using a Free Wake Lifting Line code and the CFD Navier-Stokes solver EllipSys3D [17].

Over the last 15 years, more studies have been carried out, incorporating winglets of less than 10% of relative height with respect to the blade length, resulting in power coefficient increases ranging from 2% to 8%. Chattot [18] studied the effects of blade tip modifications on wind turbine performance using an optimization code, based on a numerical vortex model. The results favoured a backward sweep, and forward dihedral and winglet (facing upstream), with a height of 10%, giving a C_P increase of 3.5% at a TSR of 5.39. Lawton and Crawford [19] used a free wake vortex-based code and concluded that a winglet facing downwind of a 5% height would result in a power increase of 2% with a 2.8% increase in thrust. Elfarra et al. [20] used CFD to solve the Reynold saveraged Navier Stokes (RANS) equations plus a genetic algorithm to optimize a winglet design of 1.5% height, 84° cant angle, 2° twist, and no apparent radius of curvature. The estimated power capture increase was 9% and a 1.3% increase in the thrust coefficient. Subsequently, using the same computational method, it was reported that winglets add aerodynamic forces and bending moments due to their weight. Cant angles of 45° and 90° were analysed, with positive and negative sweeps. Within a TSR range of 1.57.5, a 3.24.6 increase in power coefficient was estimated and 0.81.5 increase in thrust coefficient [21].

Gertz and Johnson [22] experimentally set a wind turbine baseline case for exchangeable tip designs for a 3.3 m diameter turbine. Then two winglet designs were evaluated, of 8% height, 90° cant angle, and −0.5° twist. The study showed a power increase of 5%–7% at a TSR of 6.7. Both winglets were found to have a bell-shaped power curve [23]. In a different experiment, the interaction between two wind turbines fitted with winglets was studied. The wind turbine located downstream saw a decrease in the power capture, however, the added power extraction of both was higher. Winglets had a height of 6%, 90° cant angle, 1° twist, and −0.5° sweep angle. The increase in power coefficient recorded was 4.2% at around a TSR of 6 and a 6.5% increase in thrust coefficient [24].

Mühle et al. [25] tested the effect of winglets on the tip vortex and the near wake, finding that for wake regions larger than x/D = 4.0, the wake's mean recovered faster due to the tip vortex interaction stimulated by the winglets, in addition to a higher power extraction. Winglets were designed with a height of 10.76%, a curvature radius of 3.09%, a cant angle of 90°, and a 17.86° sweep angle. At a TSR of 6, the increase in power coefficient was 10.68% and 12.64% for the thrust coefficient. The wind turbine manufacturer ENERCON is probably the only large manufacturer that has exploited the potential of winglets. An example of this is the 2010 E−126 model, an upgraded version of the 2007 E−126 model. The new model captured between 12% and 15% more energy by refining the flow around the nacelle and by adding winglets [8].

Studies on winglets for tidal turbines are scarce, with most published work based on numerical simulations. Most of the results produced a similar outcome that backwards-facing winglets should perform better. Zhu et al. [26] took power and thrust measurements from an experimental study on a horizontal axis marine turbine, carried out by Bahaj et al. [27] at the University of Southampton to adjust their baseline for their RANS simulation. Their best simulated design produced a power increase of 3.96% at a tip speed ratio of 7 and a pitch angle of 15° with a

[1] As an unwritten convention, positive cant angles face the back of the turbine and negative ones to the front, The first ones have the same orientation as winglets on aeroplane wings.

Table 1
Studies on HATs with winglets and their design parameters.

Research Paper				Parameters							Results	
Source	Type	Country	Method	Height	Radius	Cant	T, t[a]	Sweep	Aerofoil	TSR (λ)	$P_{aug.}$	$T_{aug.}$
				[%R]	[%H]	[°]	[°]	[°]			[%]	[%]
Wang et al., 2023	Tidal	China	Exp. + CFD	10		60			S809	3.5–8	5.7	
Dejene et al., 2023	Wind	Ethiopia	RANS k-ω SST	0.7		−90			S809	7.5	5–10	7–8
Bayu and Shin, 2023	Wind	Japan	CFD-RANS	1.5–5		−90,90			S809		2.21	2.02
Young et al., 2019	Tidal	UK	VLM + Exp.	10, 20	(10 mm)	−90-90				4	10	
Ren et al., 2019	Tidal	China	CFD-RANS	5.3		−90, 90			NACA63-418	4.2	4.66	
Ren et al., 2017	Tidal	China	CFD-RANS	6.3		−75-90			NACA63-418	5	4.34	3.97
Zhu et al., 2017	Tidal	China	CFD	2.5	48	−90, 90	–	45	NACA 63-812	3–10	3.96	
Ostovan and Uzol, 2016	Wind	Turkey	Exp.	6	(0)	90	1T	−0.5	PSU 94-097	~6	4.2	6.5
Elfarra, Sezer-Uzol and Akmandor, 2015	Wind	Turkey	CFD + GA	1.5	(0)	45, 90	0, 2T	+ –	S809	1.5–7.5	3.2–4.6	0.8–1.5
Lawton and Crawford, 2014	Wind	Canada	CFD	5		90	6.73T	0	NACA 64		~2	2.8
Elfarra, Sezer-Uzol and Akmandor, 2014	Wind	Turkey	CFD + GA	1.5	(0)	84	2T		S809		~9	~1.3
Gertz, Johnson and Swytink-Binnema, 2012	Wind	Canada	Exp.	8	(0)	90	−0.5T	0	PSU 94–097	6.7	5–7	
Chattot, 2009	Wind	USA	Num.	10	(0)	−90			S809	5.39	3.5	
Gaunaa and Johansen, 2007a	Wind	Denmark	Num.	2	25	90			Risø B1-15	8	2.47	2.61
Johansen and Sørensen, 2007	Wind	Denmark	CFD	2	20	90	4T	0			1.0–1.8	1.2–3.6
Johansen and Sørensen, 2006	Wind	Denmark	CFD	1.5		90		0	NACA 64-518		1.3	1.6
Shimizu et al., 2003	Wind	Japan	Exp.	9		Mie-type			NACA 4418	5.42	8.75	
van Bussel, 1990	Wind	Netherlands	Num.	20		Mie-type			NACA 4412	8	=	
Shimizu et al., 1990	Wind	Japan	Exp.	~20		Mie-type			FX74-CL6-140	4	27	
Gyatt and Lissaman, 1985	Wind	USA	Exp.	5		Single, fin, and double			NACA 23012,21		–	

[a] T: twist, t: toe angle.

dual winglet of 2.5% height, 1.2% radius, 45° sweep, and each winglet facing the pressure and suction sides with cant angles of 90°. Ren et al. [28] proposed a triangular winglet bent downstream for their RANS equations simulation. The results showed that winglets increased the power coefficient by 4.34% and the thrust coefficient by 3.97% at an optimal TSR of 5. The design had a height of 6.3%, an 18:1 elliptical tip of 10% the width of the winglet base aligned with the centreline of the blade, and a cant angle of nearly 90°. In 2019, Ren et al. [29] also compared the effect of facing the winglets upstream and downstream, finding that the best design achieved a 4.66% power increase when facing downstream at a TSR of 4.2. The triangular winglets had a height of 5.3%, with a tip-to-base proportion of 84%, and faced the suction side.

Young et al. [30] evaluated four different winglets, consisting of a linear extension of the tidal turbine blade, varying the main parameter of cant angle. Two heights were considered, 10% and 20%, and relative curvature radii of 28% and 56% respectively. In their study, the power coefficient, the hydrodynamic efficiency, and the structural efficiency were considered. After initial simulations using a vortex lattice code called Tornado, three winglets were designed to face upstream, and one downstream. In all cases it was hypothesized that blades with winglets perform better than the regular blade. However, their results showed that only the winglets facing upstream did show better performance. It was proposed that viscous effects (i.e., a separation at the corner of the blade-winglet junction) play a role in the reduction in power coefficient for the winglet facing downstream. A summary of the aforementioned studies is given in Table 1, an expanded list can be found in Ref. [31].

Most recently, Bayu and Shin [32] investigated the effect of winglets on a wind turbine using a RANS model coupled with a k-ω SST turbulence model. Their configuration included winglets facing upstream and downstream directions. Their best design had a 3%R height and a cant angle of −90° (upstream configuration) with power coefficient increases of 1–2% and thrust coefficient increasing by 1–3%. Dejene et al. [33] used a similar model to investigate the effect of winglets on the NREL Phase VI wind turbine. Winglets were 0.7%R high, facing the suction side and with cant angles of 30°, 45° and 60°. Expected power generation increase ranges from 5% to 10% with thrust coefficients increasing 7%–8%. Wang et al. [34] performed a numerical and experimental study of a tidal turbine with 10%R height and 60° bent winglet facing the direction of the current. The winglet configuration improved the efficiency by 5.7% compared to the blade extension.

In summary, to date, there has been no consensus in the literature on the best direction of winglets for horizontal axis tidal turbine blades – upstream or downstream – let alone more detailed parameters such as height and curvature radius and their performance. This work is aimed at providing more insights into the performance of a model tidal turbine with rotor blades fitted with different winglets at different configurations tested experimentally.

3. Experimental design, setup and calibration

As part of this research, several winglets were designed, manufactured, and tested to provide an understanding of the influence of varying winglet geometry on rotor thrust and power coefficients as well as act as a benchmark for future work. The model turbine used in the experiments is a 3-bladed 'upwind' horizontal axis device with a blade diameter of 1m (Fig. 3). The turbine is fully instrumented and equipped with a dynamometer that measures rotor torque and thrust at the hub. It utilises full strain gauge bridges and runs 'wet' upstream of all seals and bearings [35]. Rotor speed and blade radial position are quantified via a rotary encoder mounted on the main shaft within the nacelle. A 2-stage planetary gearbox and a synchronous generator convert mechanical energy to electrical and the rotor speed is controlled either by a wire-wound resistor bank or an electrical variable load. All data travelling out from the turbine is sampled and amplified using a wireless telemetry system to transmit data from the shaft to cables that join into a

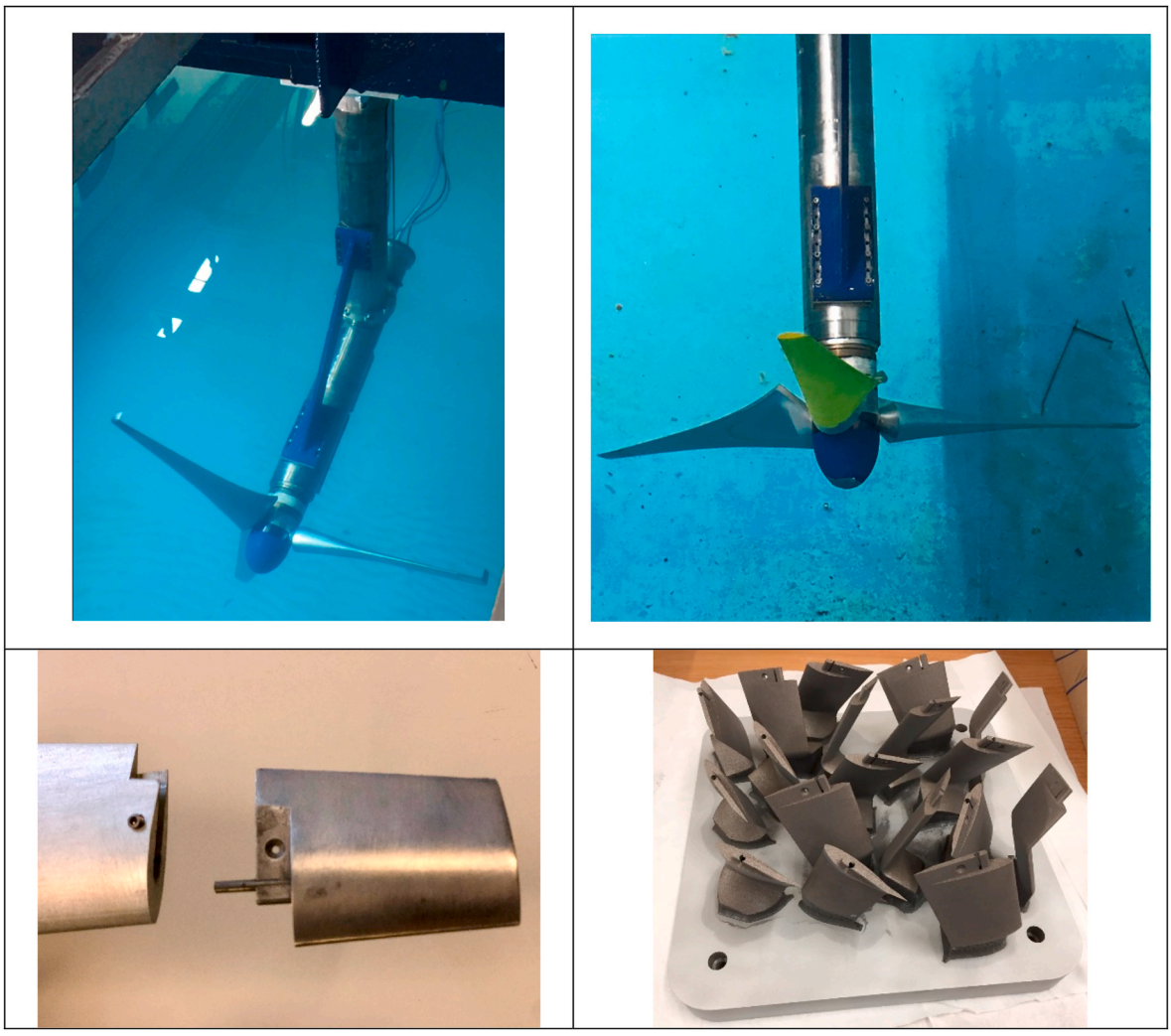

Fig. 3. Turbine installed in towing tank (Top left), main blade (Top right), blade and winglet interface (Bottom left), 3D printed winglets (Bottom right).

main umbilical cord that also conveys the generated power out and low voltage DC power in to power the onboard systems. Further details of the turbine design and general set-up can be found in Refs. [36,37]. The blade profile geometry was provided by SIMEC Atlantis Energy Ltd. under an NDA, but a full tidal turbine blade geometry can be found in Ref. [27]. The design was slightly modified to enable the tips to be interchangeable, and the turbine has the capability to adjust the blade pitch from -5° to 5° in increments of 1°.

The blades were milled on a 5-axis CNC machine at the Engineering Design and Manufacturing Centre at the University of Southampton from T6082-T6 aluminium alloy, with an accuracy of ± 50 μm. The winglets were 3D printed in aluminium at an accuracy of ± 0.1 mm, hand polished and finished.

The thrust and torque signals were collected at a frequency of 67 Hz, filtered and amplified via a wireless telemetry system located inside the nacelle. A National Instruments® data acquisition (DAQ) box, model NI USB-6210, would receive the analogue signals, pass them to a LabVIEW® program for real-time viewing, and save the data for post-processing. The power was dissipated either by using an Aim-TTi LD300 Electronic Load or a 280-W rheostat.

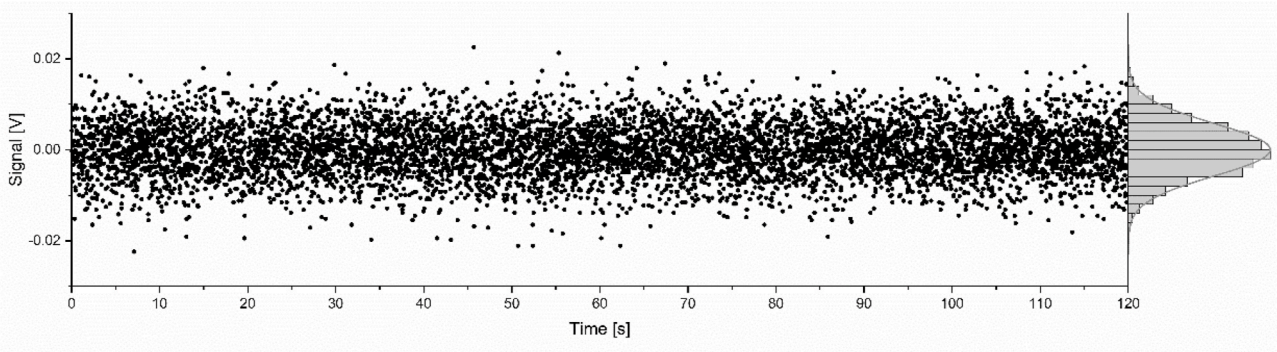

Fig. 4. Noise in the acquisition signal.

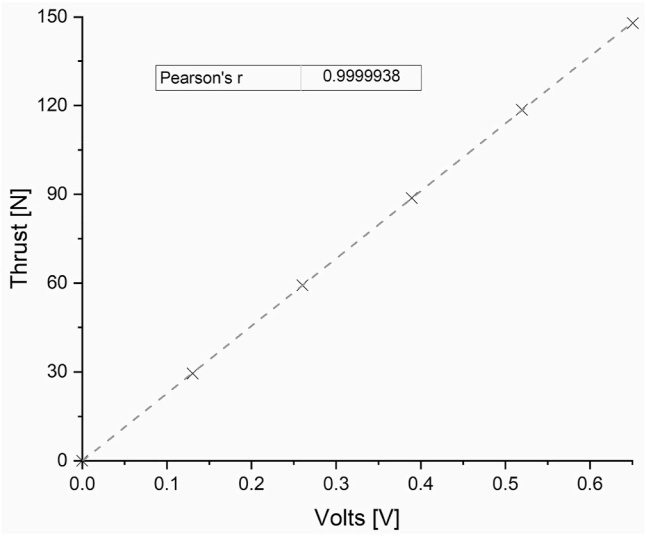

Fig. 5. Thrust calibration.

Table 2
Measurement uncertainties.

	Thrust (N)	Torque (N·m)	Ω (rmp)	Power (W)
Precision uncertainty	0.8538	0.0327	0.48	0.49
Regression uncertainty	0.4311	0.0257	–	–
Total uncertainty	0.9564	0.0416	0.48	0.49
Percentage of the mean	1.29%	0.77%	0.53%	1.30%

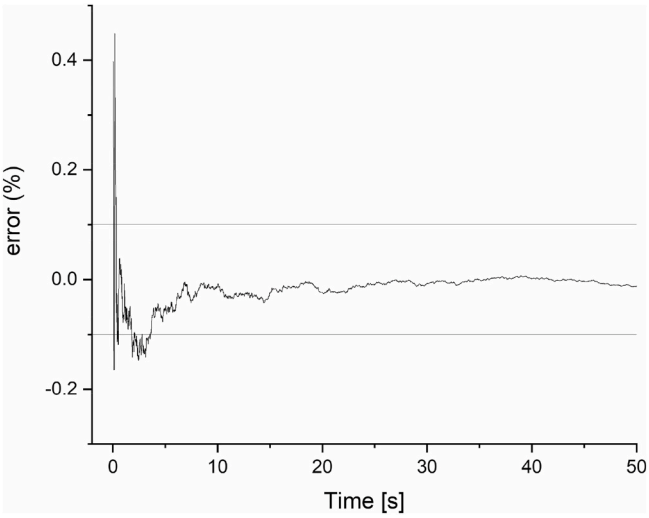

Fig. 6. Percentage error for a sample time of 2 min.

The thrust dynamometer was calibrated from 0 to 150 N at intervals of 30 N with a precision of 0.05 mN. The torque dynamometer calibration ranged from 0 to 11 N m using intervals of 2.2 N m measured to 0.02 mN m, by hanging 0.5 kg weights at 0.442 ± 0.001 m from the centre of the shaft at 0 ± 0.5° at the plane of rotation. The zero reading for the thrust has scattered noise with a normal distribution as shown in the perpendicular histogram of Fig. 4 with a standard deviation of ±5.77 mV. The linear correlation has a value of 0.9999938 as shown in Fig. 5. Measurement uncertainties are shown in Table 2. Precision has to do with the instrumentation and the regression uncertainty is derived from the calibration plot.

Averaging the signal over a period of 120s and plotting the error, the mean and the standard deviation converge with an error of less than 0.1% in just under 5 s as can be seen in Fig. 6. After performing the repeatability test, it was found that the revolutions per minute (rpm) can be estimated around a predefined value with an accuracy of ±0.48(02) rpm.

Experiments were conducted at the wave/towing tank at Solent University in Southampton, UK. The tank has dimensions of 60 m long × 3.7 m wide × 1.8 m deep. The turbine was towed at 0.76 m/s, allowing the turbine rotor to rotate within the range of 60–120 rpm. The towing speed was selected to give a sufficient range of blade Tip Speed Ratio whilst being slow enough to maximise data collection at a fixed acquisition frequency. The Froude number was approximately 0.137 (water depth 3.5m, velocity 0.76 m/s), scaled to be representative of a real tidal channel and Reynolds numbers of approximately 1.5×10^5 were observed at the tips of the blade (chord at scaled model of 0.0413 m) at an optimum rotational operation speed (TSR = 5). Towing faster resulted in minimal change in performance curves (Re. independence), whilst decreasing time for data collection due to length restriction. Depending on the winglet configuration, the rotational speeds chosen to characterise the turbine were equivalent to values ranging from 4.5 to 7.5 TSR (λ).

The following standard equations are used to present non-dimensional rotor performance:

$$C_P = \frac{Power}{\frac{1}{2}\rho A u^3} \quad \text{Equation 1}$$

$$C_T = \frac{Thrust}{\frac{1}{2}\rho A u^2} \quad \text{Equation 2}$$

$$TSR(\lambda) = \frac{\omega R}{u} \quad \text{Equation 3}$$

Where ρ is the fluid density, A is the swept area of the rotor, u is the inflow velocity, ω is the rotational speed in radians per second, and R is the rotor radius.

The characterisation of the turbine with the straight blade extensions (no winglets) for TSR from 4.5 to 7.5 is shown in Fig. 7. The average value of C_P is 0.42, and C_T is 0.78, both values quoted for further comparisons with winglets tests. Each TSR data point was obtained over a 1-min run to characterise the performance of the blades with winglets. Each run has a ramp-up period and a breaking period. In between these, a steady condition was achieved for approximately 30 s which generated over 2000 data points at a sampling rate of 67 Hz. The error bars are calculated following the measurement uncertainties defined in Table 2.

The maximum value of C_P is defined by the limit quantified by Betz [38] for a horizontal axis turbine which is equal to 16/27 or 59.3% of the available power to the swept area of the rotor. In practice, C_p is used as a global or whole-device efficiency value and is applied at the rear of the turbine incorporating electrical and drivetrain losses but here it is applied at the rotor and can be measured using the dynamometer at the hub. Tip and hub losses are significant contributors to the difference between real rotor C_p and the Betz limit [35]. Fig. 8, from formulae published by Wilson et al. (1976) [39], illustrates the effect of tip losses on rotor performance and thus efforts to reduce blade drag by minimising or completely eliminating tip losses that should be incorporated into the blade design.

The design parameters of the winglets presented herein can be seen in Table 3. The three main parameters that could be compared between winglets were height, radius of curvature, and cant angle, plus aerofoil orientation (Fig. 9). A positive cant angle means that the winglet is facing the suction side (backwards) and a negative angle that is facing the pressure side (forwards). In this study the only winglet facing the front of the turbine is winglet 7. In all cases, the distance from the hub centre to the outer part of the blade is kept at constant 0.5 m.

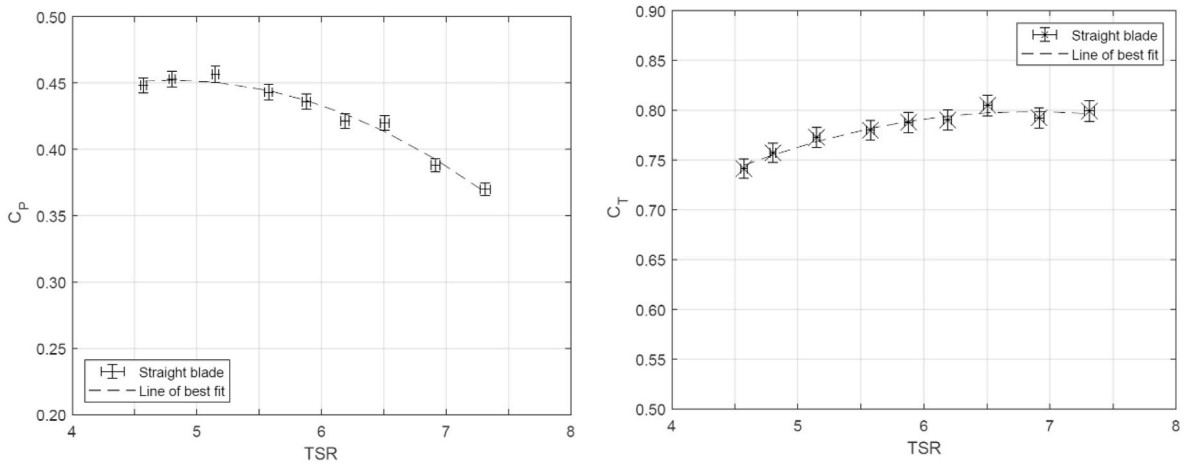

Fig. 7. Tidal turbine C_P (Top) and C_T (Bottom) curves vs. TSR.

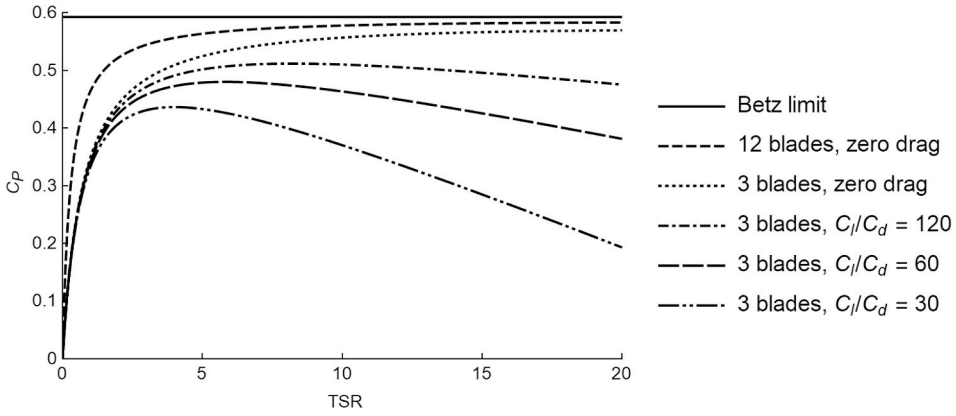

Fig. 8. The variation of C_P with design TSR for various lift/drag ratios, zero drag and number of blades, where C_l and C_d are the coefficients of lift and drag respectively.

Table 3
Design parameters for selected winglets – see also Fig. 9.

Element	Height	Radius	Cant	Aerofoil
Blade tip (T1)	0 mm (0.0%)	0%	0°	Blade
Winglet 2 (W2)	12.5 mm (2.5%)	50%	90°	Extension
Winglet 3 (W3)	25 mm (5.0%)	50%	90°	Extension
Winglet 4 (W4)	50 mm (10.0%)	50%	90°	Extension
Winglet 5 (W5)	25 mm (5.0%)	25%	90°	Extension
Winglet 6 (W6)	25 mm (5.0%)	100%	90°	Extension
Winglet 7 (W7)	25 mm (5.0%)	25%	−90°	Extension
Winglet 8 (W8)	25 mm (5.0%)	25%	90°	Inverted

4. Results and discussion

4.1. Winglet height

The first parameter to compare was winglet size. W2, W3 and W4 have a 2.5%, 5% and 10% height respectively, with a relative curvature radius of 50% (Fig. 10).

Fig. 11 shows the winglet blade performance in terms of power (C_P) and thrust (C_T) coefficients for different heights (Table 3) as a function of TSR. W2 has an average C_P value of 0.40, whilst W3 and W4 had C_P at 0.35 and 0.38 respectively. These values are lower when compared with a straight blade. Additionally, in all three cases, the thrust coefficient increased when compared with a straight blade. This was contrary to the assumption that the reduction in induced drag during turbine operation could outweigh the increase in profile drag due to the addition of winglets [20].

As can be seen in Fig. 11, in terms of power coefficient (C_P) in all cases, the blade -winglet configurations underperform compared to the straight blade. These results are in contrast to previously published numerical studies on wind turbines [16,17,19], as well as the experimental results from Ostovan and Uzol [24]. Computational simulations, specifically on tidal turbines, either supported backwards-facing winglets or found no considerable difference regarding their orientation, either facing forwards or backwards [26,29].

4.2. Winglet curvature radius

The second parameter to examine is the curvature radius. As shown in Fig. 12 W5 has a 25% radius, W3 50%, and W6 100%, all with a height of 5%.

Fig. 13 depicts the winglet performance in terms of C_P and C_T as a function of TSR, curvature and comparison with straight blade, all with different radii and at height of 5%. It can be seen from the figure that varying the radius of curvature from 25% to 50% C_P has almost identical values of 0.36 (W5) and 0.35 (W3) respectively. Whilst W6 at a 100% radius gave a relatively higher value of C_P of 0.39. In terms of C_P, all winglets still underperformed versus the straight blade. Previous studies compared the influence of the radius on the power coefficient [16,17], favouring a curvature radius of around 25%. At the design stage, the various winglets were designed with heights up to 10% and curvature radii between 20% and 50%. In this experiment, winglets with different curvature radii did not increase the power coefficient either, and there

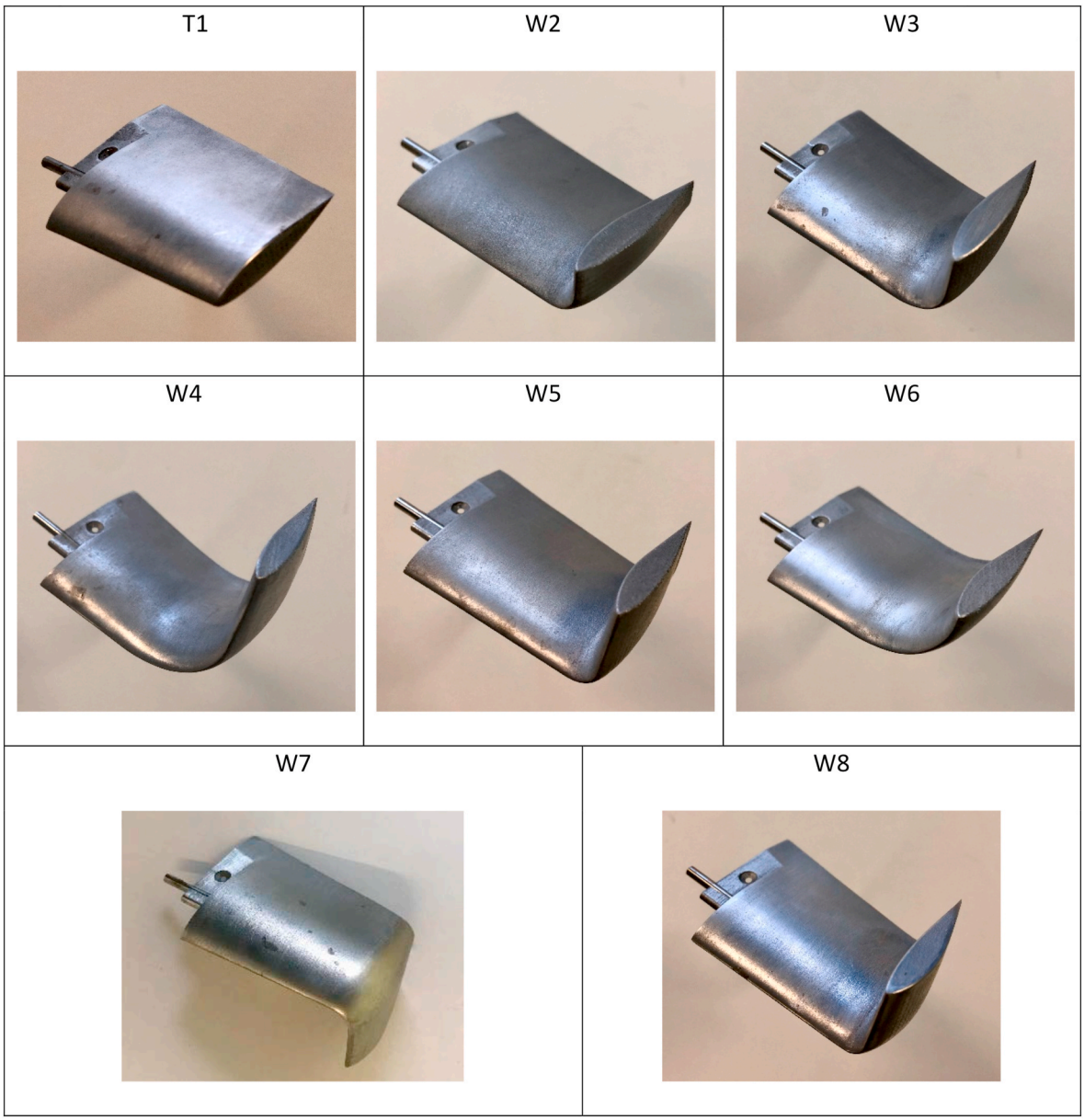

Fig. 9. Isometric view of winglets as described in Table 3. T1 is a blade tip. W2, W3, and W4 vary in height. W3, W5 and W6 have different curvature radii. W7 has an opposite cant angle but same geometry as W5. W8 has the same configuration as W5 as well but an inverted aerofoil which makes it a mirrored winglet to W7.

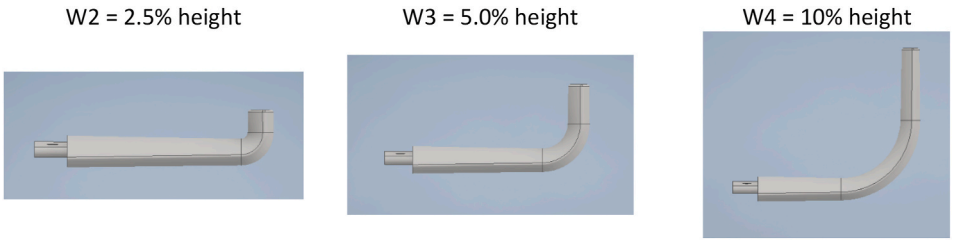

Fig. 10. Winglets 2, 3 and 4 (Table 3) with 2.5%, 5% and 10% height respectively with curvature radius of 50%.

was no evident trend found as radius increased.

4.3. Winglet cant angle

The third parameter to compare is the cant angle between W5 and W7 (Fig. 14). The design of W7 was initially carried out for completeness, as most previous studies had favoured backwards-facing winglets. In fact, it turned out to be the first winglet with an evident difference in C_P, even presenting a higher C_P than the straight blade at some regions, and eventually being key to understanding other winglets' unexpected behaviour.

Fig. 15 (Left) shows a significant difference between the power

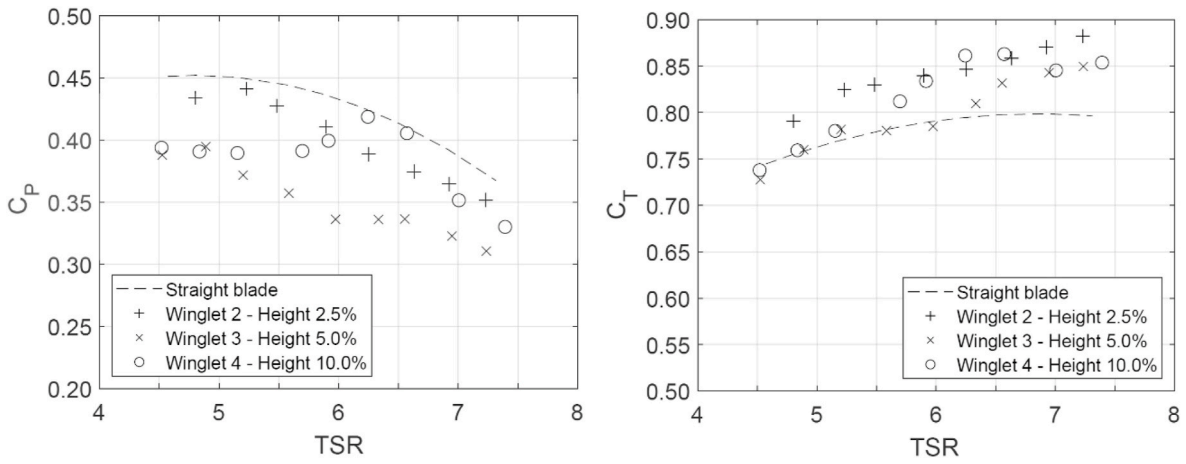

Fig. 11. Winglet performance in terms of C_P and C_T as a function of TSR, height and comparison with straight blade, all with relative radius curvature of 50%.

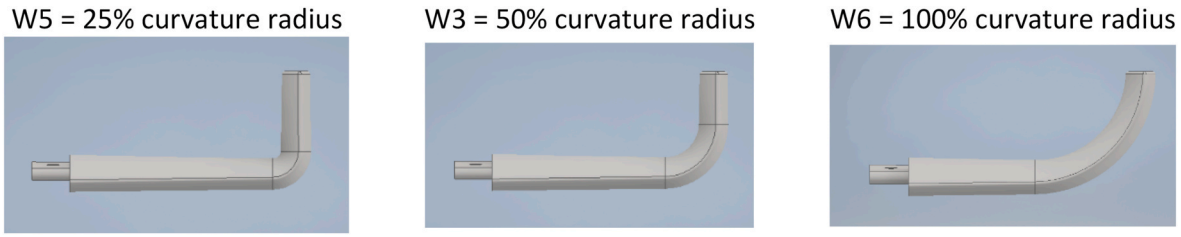

Fig. 12. Side view of winglets with same height, blade length and different curvature radii.

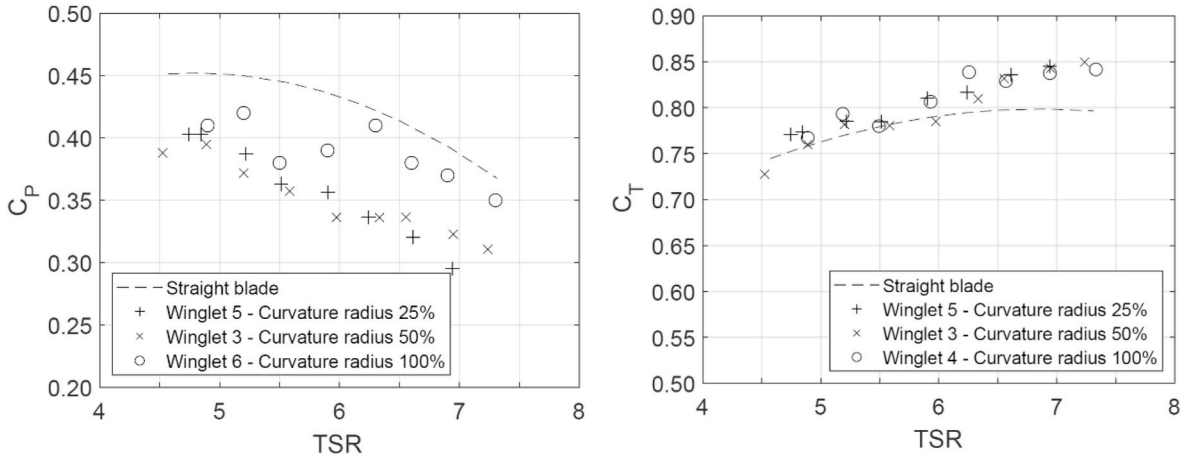

Fig. 13. Winglet performance in terms of C_P and C_T as a function of TSR, curvature and comparison with straight blade, all with different radii and 5% height.

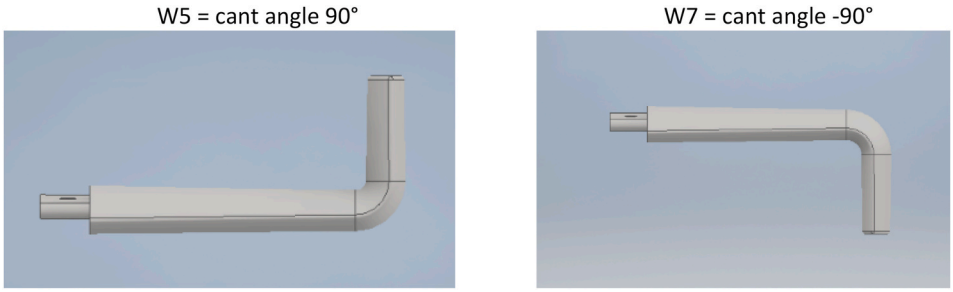

Fig. 14. Winglets facing opposite sides of the turbine, where W5 is facing the suction side and W7 towards the pressure side.

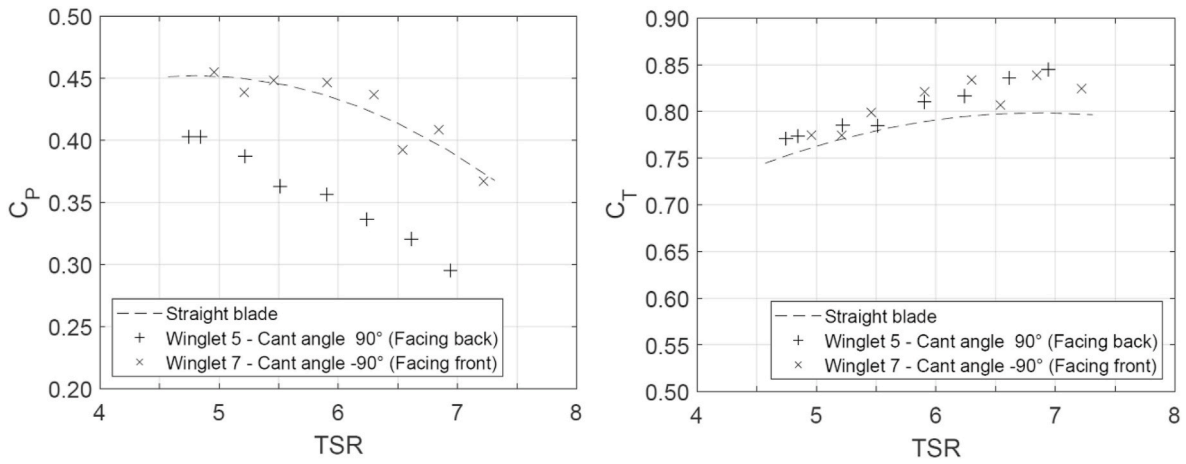

Fig. 15. Power and thrust coefficient versus TSR for winglets facing opposite sides of the rotor showing the forward-facing winglets improving C_P over backward-facing winglets and straight blade in some regions.

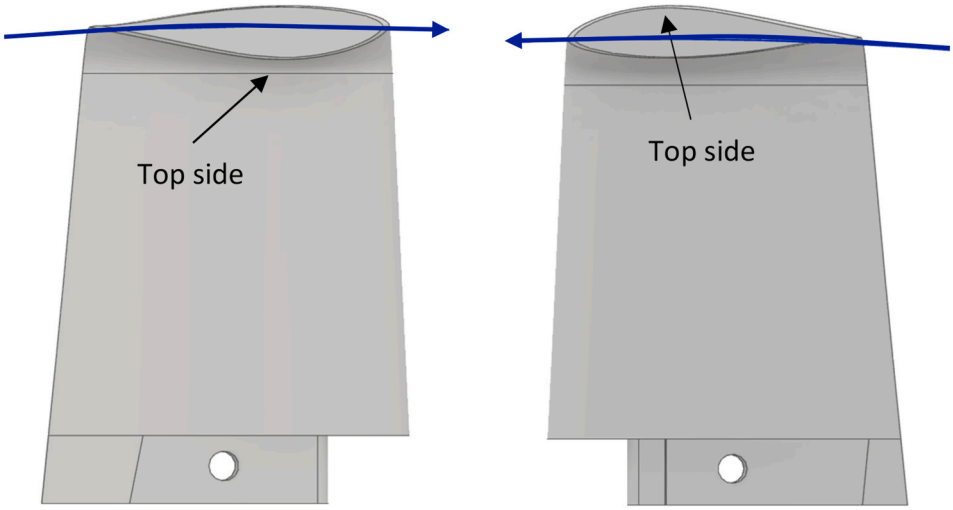

Fig. 16. aerofoil orientation for opposite cant angles and blade radius of rotation, W5 (Left), W7 (Right).

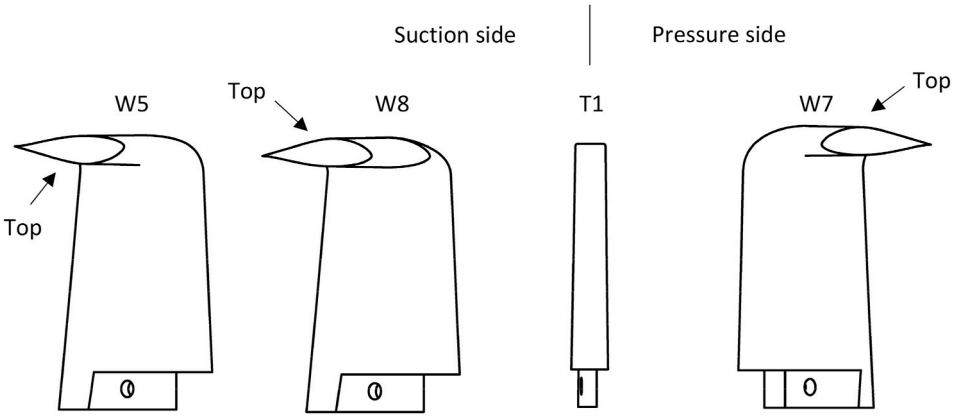

Fig. 17. Aerofoil orientation for W5, W7 and W8.

coefficient of W5, of 0.36 on average (facing the suction side), and W7 with a value of 0.42 on average (facing the pressure side), except from TSR 6 to 7 where there was an increase of 1–2%. At the same time, both thrust coefficients have an average value of 0.80 and have higher values than those of the straight blade.

In this work, W7 presented the first winglet to show an increase in performance than the straight blade (Fig. 15). It has the same geometry as W5, but it is bent upstream towards the high pressure side of the blade. The first assumption to explain this behaviour is that when winglets are bent to the back of the rotor, the aerofoil ends up being

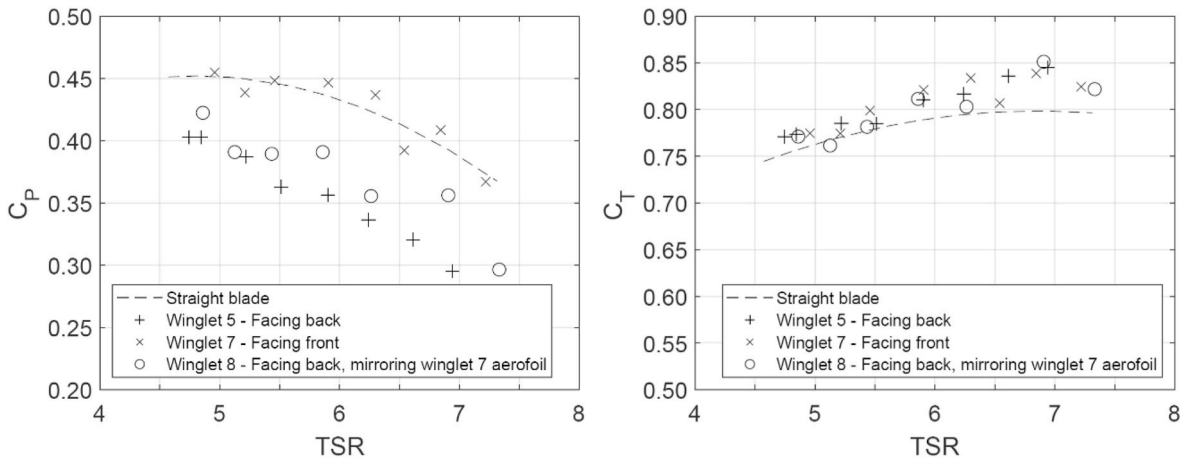

Fig. 18. C_P and C_T curves versus TSR for opposite cant angles. W7 is bent towards the front, while W5 is bent towards the back, by doing so, the aerofoils end up inversed to each other. Winglet 8 is similar to W5, with an inverted aerofoil, so it has the same orientation as W7 that is facing the front. This allows a direct comparison between cant angles for winglets facing opposite directions, as the aerofoil on both W7 and W8 have the same spatial orientation.

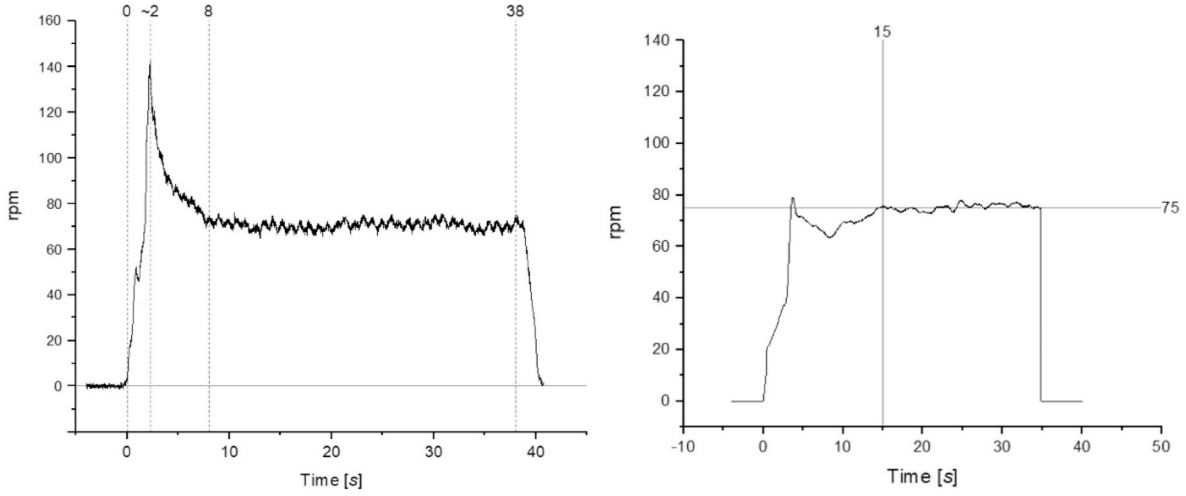

Fig. 19. Normal experimental run (Left). Modified run for flow visualisation tests (Right).

upside down (Fig. 16). It is assumed that an aerofoil rotating with such orientation would have more resistance to motion than one in an upright position.

4.4. Winglet aerofoil orientation

To compare the assumption made in the previous section, winglet W8 can be analysed. Its geometry is bent towards the back of the turbine as W5, with an inverted aerofoil. With such a configuration, the winglet ends up having a symmetrically-mirrored shape as W7 (Fig. 17).

Fig. 18, shows the results of changing the aerofoil orientation to allow a more significant comparison for the cant angle. The average C_P value of W5 is 0.36, W8 0.37 and W7 0.42. All winglets had an average C_T of 0.80. So, the difference in average C_P between W7 and W5 with opposite cant angles cannot be solely attributed to aerofoil orientation. Previous studies suggested that winglets facing the pressure side

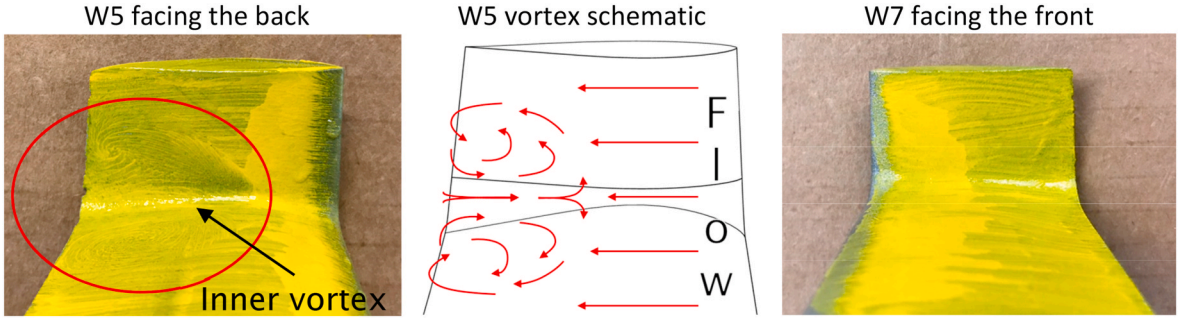

Fig. 20. Oil-based paint flow visualisation of a vortex behind winglets facing the suction side (Left), vortex schematic (Centre), and no vortex towards the pressure side (Right).

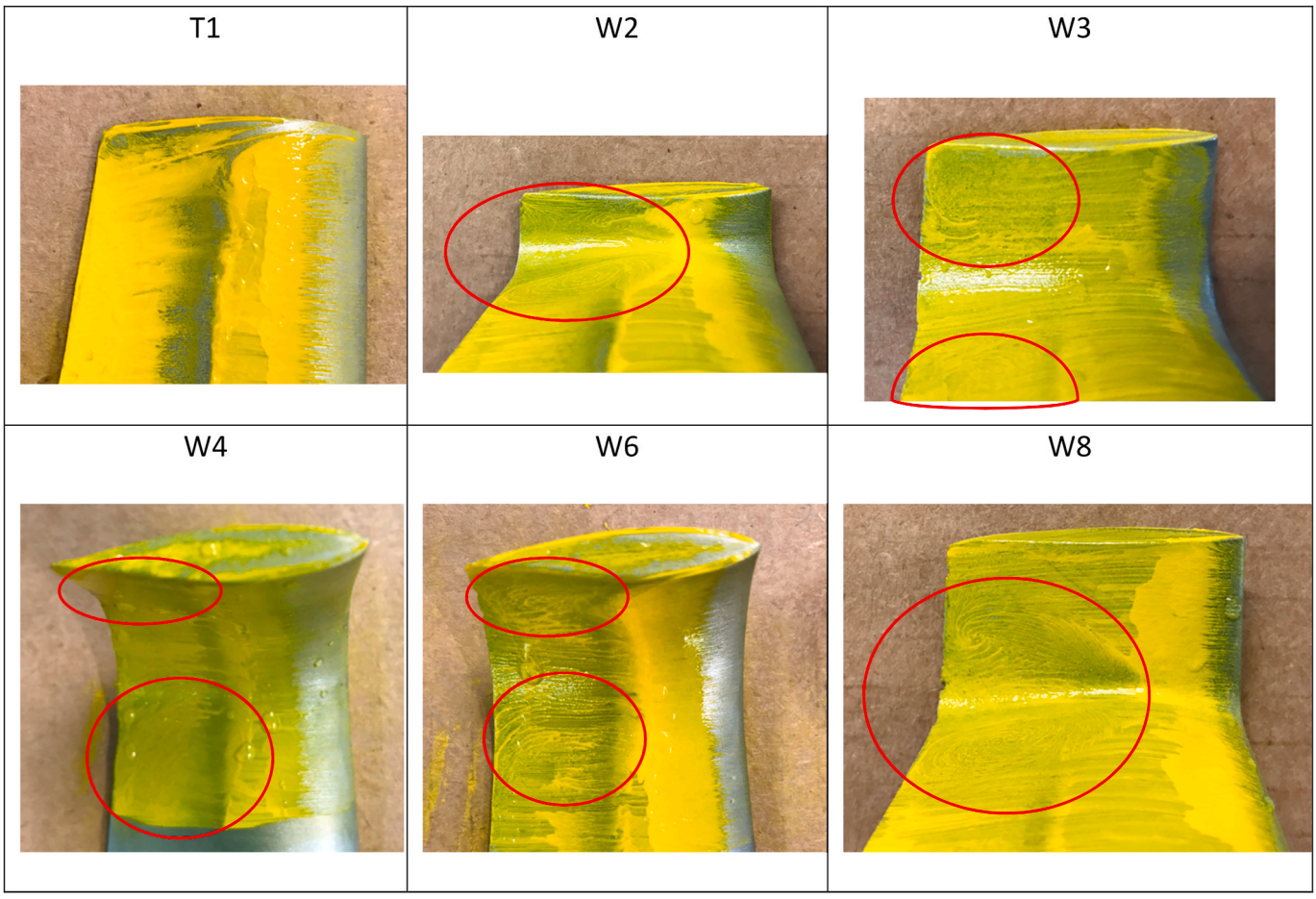

Fig. 21. Oil flow visualisation for T1 and the rest of the winglets facing the back (suction side).

performed better than the ones oriented towards the suction side, Chattot [18] with an optimization code based on a numerical vortex model, and Young [30] using a vortex lattice method.

4.5. Surface flow visualisation

Following the quantification of rotor power and thrust performance, an oil-based paint flow visualisation technique was used to study the flow on the surface of the winglets near peak C_P at a TSR of 5.0 to visualise the flow on the surface of the two symmetrical winglets W7 and W8 facing opposite directions, looking for an explanation on why W7 facing the front had a better performance than W8, which is geometrically mirrored but facing towards the back of the turbine. An example of the technique can be seen in Ref. [40]. In these experiments, oil-based paint was combined with flaxseed oil, and by trial and error a dilution ratio of 2:1 was found to have the right viscosity for a TSR of 5. Under normal testing the rotor was artificially started to overcome starting torque which resulted in a peak RPM greater than steady operation. For the runs with flow visualisation the starting procedure was modified to ensure the maximum and steady RPM only occurred during the steady operation period. Fig. 19 (Left) shows a normal test run where the carriage acceleration produces a spike in the turbine speed. Fig. 19 (Right) is the plot of the modified run to avoid such abrupt increase. It can also be noticed that the time to reach a steady speed almost doubles, steady speed time lasts less than in a normal run (as no data is processed), and instead of a gradual stop of the carriage, the turbine is left to stop on its own.

As can be seen in Fig. 20 (Left), it was identified that the phenomenon behind the underperformance of all winglets, except W7, was a vortical flow structure being formed at the blade-winglet interface. The schematic of the vortex is shown in Fig. 20 (Centre), produced by a large flow detachment from the surface. The same behaviour was found in all winglets facing the suction side (Fig. 21). That is what was impeding the winglets from enhancing the power capture and in fact reducing the power coefficient compared to a straight blade. However, in the case of W7, there was no such vortex found as can be observed in Fig. 20 (Right). All photographs were captured immediately after each run by bringing the turbine out of the water and removing the winglets.

Judging from Fig. 21, the difference in the performance of backward-facing winglets is attributed to vortices that vary in shape and size, not only per configuration but most probably for the same winglet at different speeds. Taking W2, W3 and W4, it can be seen that as the winglet increases in size, so does the vortex, with the difference that W3 and W4 seem to have either a split vortex or two of them. The more pronounced radius of curvature seems to be responsible for such an effect. A better understanding of the vortices could be achieved by using flow visualisation in 3D that includes the flow away from the winglet surface.

5. Conclusions

In recent years, numerical simulations using CFD have sought to predict the effect that blade tip winglets might have on the power and thrust coefficients of horizontal axis wind turbines. Such predictions suggested that the addition of winglets could increase the power coefficient in a range from 2% to 8%. The three main design parameters varied were height, curvature radius and cant angle. Winglet heights of up to 10% had been favoured, with relative curvature radii of around

25% and up to 50%, and a cant angle of 90° (facing the suction side). Until now only disparate experimental work has been conducted and very few studies concerning tidal turbines.

This work presents a series of experiments using a 1m-diameter 3-bladed horizontal axis tidal turbine equipped to measure rotor thrust, torque, rotational speed, and blade position. A range of winglet designs were manufactured and tested to quantify the effect of varying winglet height, radius, and cant angle. It was found that all winglet geometries tested that faced the suction side of the blade decrease the power coefficient compared to a reference straight blade. With the use of an oil-based paint flow visualisation, it was possible to identify vortical flow structures and areas of flow separation where winglets interface with the tip of the straight portion of the blade; Features that are unlikely to be simulated using inviscid numerical models.

An increase in power coefficient of 1–2% was measured for a symmetrical winglet facing the pressure side of the blade together with an increase in the thrust coefficient of up to 3–4%.

The addition of winglets could provide meaningful increases in power capture for a marginal increase in capital cost with no additional increase in rotor diameter. Adding winglets might be more favourable than increasing rotor diameter to increase power as the latter brings blades into closer proximity with sheared flow close to the seabed and wave motion near the surface and the resultant increase in dynamic loading.

This work quantifies the performance of a range of winglet designs and gives some insight into why certain designs located on the suction side of the blade underperform compared to previous numerical simulations. Numerical models that can simulate and more accurately quantify the effects of rotational flow and separation are recommended for any continuing work in this area. This work also provided some experimental evidence of enhancements of performance and to this end, further work is being planned to expand the range of winglets that can be used and to explore additional geometric properties including winglets orientated upstream on the pressure side of the blade.

CRediT authorship contribution statement

Rodolfo Olvera-Trejo: Conceptualization, Data curation, Formal analysis, Funding acquisition, Investigation, Methodology, Project administration, Software, Validation, Visualization, Writing – original draft, Writing – review & editing. **Luke Myers:** Conceptualization, Funding acquisition, Investigation, Methodology, Project administration, Resources, Supervision, Validation, Visualization, Writing – original draft, Writing – review & editing. **Luke Blunden:** Supervision, Writing – original draft, Software, Visualization. **AbuBakr S. Bahaj:** Funding acquisition, Project administration, Resources, Supervision, Validation, Writing – review & editing.

Declaration of competing interest

The authors declare that they have no known competing financial interests or personal relationships that could have appeared to influence the work reported in this paper.

Data availability

Winglets (Original data) (doi)

Acknowledgements

This research was carried out through PhD level support from the Department of Energy in Mexico (SENER), which fund was managed by the Mexican National Council of Science and Technology (CONACyT) on energy sustainability CONACyT-SENER. The research is also part of the activities of the Energy and Climate Change Division and the Sustainable Energy Research Group (www.energy.soton.ac.uk), Faculty of Engineering and Physical Sciences, University of Southampton, Southampton, SO16 7QF, UK. We kindly thank Atlantis Resources Ltd., now Proteus Marine Renewables Ltd., for providing the blade profile geometry. We also acknowledge Prof. Stephen Turnock for his encouragement on the exploration of the flow around the winglets, and Dr. Roeland de Kat for his guidance on paint-based surface flow visualisation.

References

[1] UK Government, National renewable energy action plan for the United Kingdom, 1–160, https://www.gov.uk/government/uploads/system/uploads/attachment_data/file/47871/25-nat-ren-energy-action-plan.pdf, 2010. (Accessed 11 August 2022).
[2] European Commission, Plan REPowerEU, 21, https://ec.europa.eu/commission/presscorner/detail/en/IP_22_3131, 2022. (Accessed 11 August 2022).
[3] UK Government, British energy security strategy. https://assets.publishing.service.gov.uk/government/uploads/system/uploads/attachment_data/file/1069969/british-energy-security-strategy-web-accessible.pdf, 2022. (Accessed 11 August 2022).
[4] A.S. Bahaj, Generating electricity from the oceans, Renew. Sustain. Energy Rev. 15 (2011) 3399–3416, https://doi.org/10.1016/j.rser.2011.04.032.
[5] A.S. Bahaj, Marine current energy conversion: the dawn of a new era in electricity production, Philosoph. Transact. Royal Soci. 371 (2013), https://doi.org/10.1098/rsta.2012.0500.
[6] BEIS, Contracts for difference allocation round 4 results, 1–9, https://assets.publishing.service.gov.uk/government/uploads/system/uploads/attachment_data/file/1088875/contracts-for-difference-allocation-round-4-results.pdf, 2022. (Accessed 11 August 2022).
[7] Annual report 2019, Ocean Energy Systems, 2019, p. 152. https://tethys.pnnl.gov/publications/ocean-energy-systems-annual-report-2019. August 11, 2022.
[8] E. de Vries, Close up - Enercon, Super Turbines and beyond, Windpower Monthly, 2010. https://www.windpowermonthly.com/article/1047013/close-enercon-super-turbines-beyond. (Accessed 11 August 2022).
[9] R.T. Whitcomb, A Design Approach and Selected Wind Tunnel Results at High Subsonic Speeds for Wing-Tip Mounted Winglets, Nasa Tn D-8260, 1976, pp. 1–33. https://ntrs.nasa.gov/archive/nasa/casi.ntrs.nasa.gov/19760019075.pdf. (Accessed 11 August 2022).
[10] M.D. Maughmer, Design of winglets for high-performance sailplanes, J. Aircraft 40 (2003) 1099–1106, https://doi.org/10.2514/2.7220.
[11] G.W. Gyatt, P.B.S. Lissaman, Development and testing of tip devices for horizontal axis wind turbines. https://ntrs.nasa.gov/search.jsp?R=19860009304, 1985. (Accessed 11 August 2022).
[12] Y. Shimizu, G.J. Van Bussel, S. Matsumura, A. Bruining, K. Kikuyama, Y. Hasegawa, Studies on horizontal Axis wind turbines with tip attachments. Proc. Of European Community Wind Energy Conference, 1990, pp. 279–283.
[13] G.J.W. van Bussel, A Momentum Theory for Winglets on Horizontal axis Windturbine Rotors and Some Comparison with Experiments, 4th IEA Symp. On the Aerodynamics of Wind Turbines, 1990.
[14] Y. Shimizu, E. Ismaili, Y. Kamada, T. Maeda, Power augmentation of a HAWT by Mie-type tip vanes, considering wind tunnel flow visualisation, blade-aspect ratios and Reynolds number, Wind Eng. 27 (2003) 183–194, https://doi.org/10.1260/030952403769016663.
[15] J. Johansen, N. Sørensen, Aerodynamic Investigation of Winglets on Wind Turbine Blades Using CFD, Riso-R-1543(EN), 2006, p. 1543.
[16] J. Johansen, N. Sørensen, Numerical analysis of winglets on wind turbine blades using CFD. European Wind Energy Conference and Exhibition, 2007.
[17] M. Gaunaa, J. Johansen, Determination of the maximum aerodynamic efficiency of wind turbine rotors with winglets, J Phys Conf Ser 75 (2007) 012006, https://doi.org/10.1088/1742-6596/75/1/012006.
[18] J.-J. Chattot, Effects of blade tip modifications on wind turbine performance using vortex model, Comput. Fluids 38 (2009) 1405–1410, https://doi.org/10.1016/j.compfluid.2008.01.022.
[19] S. Lawton, C. Crawford, Investigation and optimization of blade tip winglets using an implicit free wake vortex method, J Phys Conf Ser 524 (2014) 012033, https://doi.org/10.1088/1742-6596/524/1/012033.
[20] M.A. Elfarra, N. Sezer-Uzol, İ.S. Akmandor, NREL VI rotor blade: numerical investigation and winglet design and optimization using CFD, Wind Energy 17 (2014) 605–626, https://doi.org/10.1002/we.1593.
[21] M.A. Elfarra, N. Sezer-Uzol, İ.S. Akmandor, Investigations on blade tip tilting for hawt rotor blades using CFD, Int. J. Green Energy 12 (2015) 125–138, https://doi.org/10.1080/15435075.2014.889007.
[22] D. Gertz, D.A. Johnson, An evaluation testbed for wind turbine blade tip designs-baseline case, Int. J. Energy Res. 35 (2011) 1360–1370, https://doi.org/10.1002/er.1897.
[23] D. Gertz, D. Johnson, N. Swytink-Binnema, An evaluation testbed for wind turbine blade tip designs - winglet results, Wind Eng. 36 (2012) 389–410, https://doi.org/10.1260/0309-524X.36.4.389.
[24] Y. Ostovan, O. Uzol, Experimental study on the effects of winglets on the performance of two interacting horizontal Axis model wind turbines, J Phys Conf Ser 753 (2016) 022015, https://doi.org/10.1088/1742-6596/753/2/022015.
[25] F. Mühle, J. Bartl, T. Hansen, M.S. Adaramola, L. Sætran, An experimental study on the effects of winglets on the tip vortex interaction in the near wake of a model

wind turbine, Wind Energy 23 (2020) 1286–1300, https://doi.org/10.1002/we.2486.
[26] B. Zhu, X. Sun, Y. Wang, D. Huang, Performance characteristics of a horizontal axis turbine with fusion winglet, Energy 120 (2017) 431–440, https://doi.org/10.1016/j.energy.2016.11.094.
[27] A.S. Bahaj, A.F. Molland, J.R. Chaplin, W.M.J. Batten, Power and thrust measurements of marine current turbines under various hydrodynamic flow conditions in a cavitation tunnel and a towing tank, Renew. Energy 32 (2007) 407–426, https://doi.org/10.1016/j.renene.2006.01.012.
[28] Y. Ren, B. Liu, T. Zhang, Q. Fang, Design and hydrodynamic analysis of horizontal axis tidal stream turbines with winglets, Ocean Eng. 144 (2017) 374–383, https://doi.org/10.1016/j.oceaneng.2017.09.038.
[29] Y. Ren, B. Liu, T. Zhang, Influences of winglets on the hydrodynamic performance of horizontal axis current turbines, Appl. Ocean Res. 92 (2019) 101931, https://doi.org/10.1016/j.apor.2019.101931.
[30] A.M. Young, A.S.M. Smyth, V. Bajpai, R.F. Augarde, J.R. Farman, C.L. Sequeira, Improving tidal turbine efficiency using winglets, in: 13th European Wave and Tidal Energy Conference 2019, 2019, pp. 1–11.
[31] R. Olvera Trejo, An Experimental Study on the Effects of Winglets on the Performance of Horizontal axis Tidal Turbines, University of Southampton, 2022.
[32] B.K. Wardhana, B.R. Shin, Numerical investigation of the effect of winglet configurations on the blade performance for horizontal AXIS wind turbine, in: Proceeding of 8th Thermal and Fluids Engineering Conference (TFEC), 2023, pp. 783–786, https://doi.org/10.1615/TFEC2023.eet.045960. Begellhouse, Connecticut.
[33] G. Dejene, V.R. Ancha, A. Bekele, NREL Phase VI wind turbine blade tip with S809 airfoil profile winglet design and performance analysis using computational fluid dynamics, Cogent Eng 11 (2024), https://doi.org/10.1080/23311916.2023.2293562.
[34] Y. Wang, B. Guo, F. Jing, Y. Mei, Hydrodynamic performance and flow field characteristics of tidal current energy turbine with and without winglets, J. Mar. Sci. Eng. 11 (2023) 2344, https://doi.org/10.3390/jmse11122344.
[35] T. Blackmore, L.E. Myers, A.S. Bahaj, Effects of turbulence on tidal turbines: implications to performance, blade loads, and condition monitoring, International Journal of Marine Energy 14 (2016) 1–26, https://doi.org/10.1016/j.ijome.2016.04.017.
[36] A.S. Bahaj, L.E. Myers, Shaping array design of marine current energy converters through scaled experimental analysis, Energy 59 (2013) 83–94, https://doi.org/10.1016/j.energy.2013.07.023.
[37] P.W. Galloway, L.E. Myers, A.B.S. Bahaj, Quantifying wave and yaw effects on a scale tidal stream turbine, Renew. Energy 63 (2014) 297–307, https://doi.org/10.1016/j.renene.2013.09.030.
[38] A. Betz, Das maximum der theoretisch moglichen Auswendung des Windes durch Windmotoren, Zeitschrift Fur Gesamte Turbinewesen 26 (1920).
[39] J.F. Manwell, J.G. McGowan, A.L. Rogers, Wind Energy Explained: Theory, Design and Application, Wiley, 2010.
[40] C.M. Harwood, Y.L. Young, S.L. Ceccio, Ventilated cavities on a surface-piercing hydrofoil at moderate Froude numbers: cavity formation, elimination and stability, J. Fluid Mech. 800 (2016) 5–56.